J. Fluid Mech. (2016), *vol.* 803, *pp.* 275–291.
doi:10.1017/jfm.2016.469

Current generation by deep-water breaking waves

N. E. Pizzo[1,†], Luc Deike[1] and W. Kendall Melville[1]

[1]Scripps Institution of Oceanography, University of California, San Diego, La Jolla, CA 92093-0213, USA

(Received 15 October 2015; revised 11 June 2016; accepted 8 July 2016; first published online 22 August 2016)

We examine the partitioning of the energy transferred to the water column by deep-water wave breaking; in this case between the turbulent and mean flow. It is found that more than 95 % of the energy lost by the wave field is dissipated in the first four wave periods after the breaking event. The remaining energy is in the coherent vortex generated by breaking. A scaling argument shows that the ratio between the energy in this breaking generated mean current and the total energy lost from the wave field to the water column due to breaking scales as $(hk)^{1/2}$, where hk is the local slope at breaking. This model is examined using direct numerical simulations of breaking waves solving the full two-phase air–water Navier–Stokes equations, as well as the limited available laboratory data, and good agreement is found for strong breaking waves.

Key words: air/sea interactions, wave breaking, waves/free-surface flows

1. Introduction

The flow induced by deep-water wave breaking is characterized by the generation of turbulence and a coherent vortex associated with the mean flow. In the case of quasi-two-dimensional breaking, it is a line vortex ending at the lateral boundaries of the flow (Rapp & Melville 1990; Melville, Veron & White 2002; Pizzo & Melville 2013). For three-dimensional deep-water breaking, it is a half-vortex ring with dipolar vorticity at the surface (Peregrine 1999). Vortex rings are defined by their integral properties (Linden & Turner 2001), so that we can connect the circulation in this breaking-induced half-ring vortex with the hydrodynamical impulse necessary to generate it (Lamb 1932). By connecting this impulse with the momentum flux (and subsequently the energy) lost from the wave field due to breaking, we can describe the energy in the mean flow vortex in terms of the characteristic variables of the breaking wave and obtain a simple model for the ratio of the energy in the breaking-induced current to the total energy lost by breaking. That is the focus of this paper.

Breaking waves transfer momentum and energy from the quasi-irrotational surface wave field to the rotational underlying currents (Phillips 1977; Melville 1996). A better understanding of this process is crucial for an improved description of air–sea interaction, especially for coupled ocean–atmosphere models (Cavaleri, Fox-Kemper & Hemer 2012). Breaking waves, however, are two-phase turbulent flows, making

† Email address for correspondence: npizzo@ucsd.edu

detailed theoretical analysis very difficult. Therefore, numerical and laboratory studies are invaluable for gaining knowledge about these processes. Based on fundamental fluid dynamics and experiments, simple scaling models can be developed and are useful for understanding the physics of the observed integral properties of the breaking-induced flow.

Drazen, Melville & Lenain (2008) studied the breaking strength parameter b, associated with the energy dissipation rate per unit length of breaking crest ϵ_l (see also Duncan 1981; Phillips 1985) and based on an inertial scaling model for plunging breaking waves, they found

$$\epsilon_l = b\frac{\rho c^5}{g}; \quad b = \beta(hk)^{5/2}, \tag{1.1a,b}$$

with ρ the density of water, c the phase velocity, h the height of the wave at breaking, k the wavenumber and β an order-one scaling constant. The first relationship in (1.1) was proposed by Duncan (1981, see also Phillips 1985), but b was taken to be a constant. Drazen *et al.* (2008) then extended this relationship to account for the dependence of b on the local slope at breaking.

Based on this work, Romero, Melville & Kleiss (2012) compared the model given in (1.1) with existing laboratory data by equating b with the maximum slope (according to linear theory) at breaking, S, along with a threshold for breaking S_0; that is, $b = \beta(S - S_0)^{5/2}$. (Note, Drazen *et al.* (2008, figure 15) found $(hk) \approx S$ to within the scatter of the data.) Excellent agreement with the existing laboratory data was found, with b ranging over three orders of magnitude, which included both gently spilling and plunging breaking waves (Drazen *et al.* 2008, see also Romero *et al.* 2012, Grare *et al.* 2013). The agreement of the model with measurements of the dissipation of gently spilling breaking waves was surprising, as the scaling argument used to derive the model was based on the geometry of a plunging breaking wave. This prompted Deike, Popinet & Melville (2015) to numerically examine the energy dissipation rate of gravity–capillary waves using a direct numerical simulation of the two-phase Navier–Stokes equations. They found that the model continued to agree with the data, even for waves that were dissipating energy mostly through the formation of parasitic capillary waves (see also Melville & Fedorov 2015).

Next, we recall that a coherent vortex characterizes the wave breaking induced ensemble-averaged velocity field in quasi two-dimensional focusing wave breaking laboratory experiments (Rapp & Melville 1990; Melville *et al.* 2002). This vortex is the mean flow induced by breaking and it is observed to be robust, lasting more than 50 wave periods after the breaking event (Rapp & Melville 1990; Melville *et al.* 2002; Pizzo & Melville 2013). This led Sullivan, McWilliams & Melville (2004, see also Sullivan, McWilliams & Melville 2007) to parameterize the bulk effects of a breaking wave on the ensemble-averaged flow by an impulsive body force. By performing a direct numerical simulation of the Navier–Stokes equations for the fluid response to this body force model, they were able to reproduce the characteristic flow observed in the laboratory.

Pizzo & Melville (2013) used similar arguments to those of Drazen *et al.* (2008) to propose a scaling model for the circulation, Γ, induced by both plunging and spilling breaking waves. They found

$$\Gamma = \gamma_0\frac{(hk)^{3/2}c^3}{g}, \tag{1.2}$$

with γ_0 an order-one scaling constant. The model was shown to be in agreement with the limited available laboratory data. We will further examine this relationship numerically in this paper. Finally, the arguments in their paper also served to clarify the agreement that was found by Romero *et al.* (2012, see also Grare *et al.* 2013, Deike *et al.* 2015) for the scaling of b for both plunging and spilling breaking waves.

The paper is organized as follows. Section 2 discusses the dynamics of the breaking event and we derive the scaling model for the energy remaining in the vortex induced by breaking. Section 3 examines this model through direct numerical simulations of the two-phase Navier–Stokes equations. Section 4 presents the conclusions and implications.

2. The impulse and energy in the post-breaking mean flow

In this section we examine the impulse and energy needed to generate the half-ring vortex induced by breaking, and compare this to the momentum and energy flux lost from the wave field by the breaking event. This will yield a scaling model for the amount of energy remaining in the mean flow after a breaking event.

The basic methodology follows laboratory experiments on dispersive focusing breaking waves (Rapp & Melville 1990), where a control volume analysis is performed. These integrals make it possible to exploit the linearity of the wave field, which is valid far from the breaking region, to deduce integral properties of the flow induced by breaking. These properties can then be easily measured in numerical and laboratory experiments, using only the geometry of the free surface.

2.1. *Properties of the flow induced by wave breaking*

Consider a unidirectional wave group that propagates in the x direction, with y denoting the transverse direction and z pointed upwards. Our system is governed by the Navier–Stokes equation,

$$\frac{\partial \boldsymbol{u}}{\partial t} + \boldsymbol{u}\cdot\nabla\boldsymbol{u} = -\frac{1}{\rho}\nabla p + \nu\nabla^2\boldsymbol{u} + \boldsymbol{g}, \tag{2.1}$$

where $\boldsymbol{g} = -g\hat{\boldsymbol{z}}$ ($\hat{\boldsymbol{z}}$ denotes the unit vector in the vertical direction) is the acceleration due to gravity, ρ the density of water and ν the fluid viscosity.

A conspicuous feature of the focusing wave packets sketched in figure 1 is that there is a natural separation between the waves and the breaking-induced flow. We will exploit this fact by forming integral relationships for the properties of the waves and the induced flow that obey simple sum relationships. That is, the waves rapidly propagate out of the region of breaking, so that we assume there is no subsequent interaction between them and the induced flow. Furthermore, we assume that any permanent exchange of momentum and energy from the wave field to the water column is confined to the region of breaking.

First, we consider the energy balance. To this end, we take the inner product of $\boldsymbol{u}$ with (2.1) and integrate over a control volume V and time $\mathcal{T}_0$. The control volume V (with a boundary denoted as $\mathcal{A}$) is chosen so that all of the effects that we are describing, due to breaking, occur well within this domain. In particular, we integrate over a depth $(-\infty, \eta)$ and a horizontal domain $(\boldsymbol{x}_1, \boldsymbol{x}_2)$. The horizontal domain is chosen so that the wave field is linear at the locations x_1 and x_2, and the transverse direction has a range from $(-\Lambda/2, \Lambda/2)$, where Λ is the scale of the wave in the transverse direction. Note, the dispersive focusing laboratory experiments discussed in

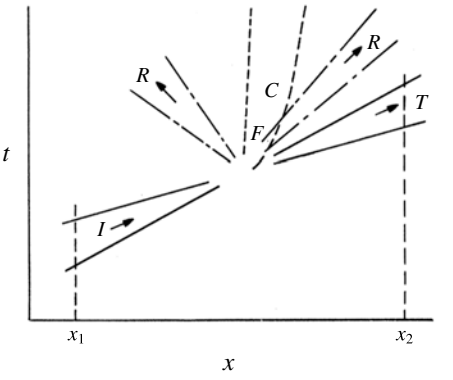

FIGURE 1. A schematic of the focusing wave groups considered in this paper, from Rapp & Melville (1990). The incident wave group, I, focuses at F, radiating, R, and transmitting, T, waves away from this region. In the area of breaking, currents, C, and turbulence will be generated. Far upstream and downstream of the breaking region, (x_1, x_2) respectively, the waves are approximately linear.

this paper are quasi two-dimensional, which corresponds to $\Lambda \to \infty$. Furthermore, the (turbulent and mean) flow generated by breaking are bound to this region and do not transport integral quantities out of this volume.

Therefore, we find (Phillips 1977; Mei 1989; Rapp & Melville 1990)

$$\int_V \frac{1}{2}\rho(u_i u_i)|_{t=0}^{t=\mathcal{T}_0}\,\mathrm{d}V + \int_0^{\mathcal{T}_0}\int_A \left(\frac{1}{2}\rho u_i u_i + p + \rho g z\right)\Big|_{x_1}^{x_2} u\,\mathrm{d}A\,\mathrm{d}t = \int_0^{\mathcal{T}_0}\int_V \rho\epsilon\,\mathrm{d}V\,\mathrm{d}t, \tag{2.2}$$

where $\boldsymbol{n}$ is a unit vector normal to the surface $\mathcal{A}$, ϵ is the rate of dissipation and Einstein summation over repeated indices is employed.

Now, at times $t = 0$ and $t = \mathcal{T}_0$, there are no waves or turbulence (following laboratory experiments (Rapp & Melville 1990; Melville *et al.* 2002; Drazen & Melville 2009) where we have assumed that the remaining energy, several wave periods after breaking, is contained entirely in the mean vortex flow) in the volume V. Therefore, we find $(u_i u_i)|_{t=0}^{t=\mathcal{T}_0} = \overline{\boldsymbol{u}}(\mathcal{T}_0)\cdot\overline{\boldsymbol{u}}(\mathcal{T}_0)$ with $\overline{\boldsymbol{u}}$ denoting the mean flow current. Furthermore, as the flow induced by breaking is confined to the interior of V, the flux term will be solely due to the waves. Finally, we average over the wave period T (we denote this average by angled brackets), and conclude

$$\mathcal{E}_c + \mathcal{D} + \Delta\mathcal{F} = 0, \tag{2.3}$$

where $\mathcal{E}_c$ is the (averaged) energy in the mean flow, defined as

$$\mathcal{E}_c = \left\langle \int_V \frac{1}{2}\rho\overline{\boldsymbol{u}}\cdot\overline{\boldsymbol{u}}\,\mathrm{d}V \right\rangle, \tag{2.4}$$

while $\Delta\mathcal{F} = \mathcal{F}(x_2) - \mathcal{F}(x_1)$ is the long time integrated change in energy flux, given by

$$\mathcal{F} = \left\langle \int_0^{\mathcal{T}_0}\int_{-\infty}^{\eta}\int_{-\Lambda/2}^{\Lambda/2} \left(p + \frac{1}{2}\rho(\nabla\phi)^2 + \rho g z\right)\phi_x\,\mathrm{d}z\,\mathrm{d}y\,\mathrm{d}t \right\rangle, \tag{2.5}$$

and the dissipation $\mathcal{D}$ is given by

$$\mathcal{D} = \left\langle \int_0^{\mathcal{T}_0} \int_V \rho\epsilon \, \mathrm{d}V \, \mathrm{d}t \right\rangle. \tag{2.6}$$

In this paper we will examine the ratio of $\mathcal{E}_c$ and $|\Delta\mathcal{F}|$, which will serve to compare the energy in the mean flow to the total energy lost by the wave packet. In order to do so, we must quantify the energy in the mean flow as a function of the variables characterizing the breaking wave field.

To this end, we next perform a control volume analysis of the momentum budget. Analogous to our energy budget, we integrate the x-component of equation (2.1) over the region V, and over a duration $\mathcal{T}_0$, to find

$$\left\langle \int_V \rho u(\mathcal{T}_0) \, \mathrm{d}V \right\rangle + \Delta\mathcal{S} = 0, \tag{2.7}$$

where $\Delta\mathcal{S} = \mathcal{S}(x_2) - \mathcal{S}(x_1)$ is the long time integrated momentum flux (or radiation stress), and is given by

$$\mathcal{S} = \left\langle \int_0^{\mathcal{T}_0} \int_{-\infty}^{\eta} \int_{-\Lambda/2}^{\Lambda/2} (\rho u^2 + p) \, \mathrm{d}z \, \mathrm{d}y \, \mathrm{d}t \right\rangle. \tag{2.8}$$

Recall, the velocity $\boldsymbol{u}$ remaining in V at time $\mathcal{T}_0$ is solely due to the mean flow induced by breaking, i.e. $\boldsymbol{u} = \overline{\boldsymbol{u}}$. The second term in (2.7) is due to changes in the momentum flux of the wave groups, and has a simple solution for linear waves (Longuet-Higgins & Stewart 1964; Phillips 1977). Note, this quantity is in general non-zero for wave groups, unlike the wave momentum (Longuet-Higgins & Stewart 1964; McIntyre 1981).

Next, based on the laboratory experiments, we assume that the momentum flux lost by the wave field goes entirely into the mean flow. That is, although some of the momentum lost from the wave field due to breaking will propagate away from the region in the form of surface waves, Rapp & Melville (1990) found that the energy in these radiated waves was much less than the total energy lost by breaking. Therefore, for now we ignore this effect.

Our integral momentum balance becomes

$$\left\langle \int_V \rho\overline{u} \, \mathrm{d}V \right\rangle = |\Delta\mathcal{S}|. \tag{2.9}$$

Now, as these waves are linear at locations x_1 and x_2, we can easily compute the integrals given in terms of the wave energy. From Longuet-Higgins & Stewart (1964), we have $\mathcal{S}(x_i) = F(x_i)/2c_{gi}$ where the group velocity $c_g = \omega/2k$ for ω the angular frequency and k the wavenumber. Following Drazen *et al.* (2008, see also Pizzo & Melville (2016)), we assume that $c_g \equiv c_g(x_2) = c_g(x_1)(1 + O(S))$, where we recall S is the linear prediction of the maximum slope at breaking. This was found to be experimentally true to within 5 %–10 % (see § 3.1.1 Tian, Perlin & Choi 2011). Therefore, we have $|\Delta\mathcal{S}| = |\Delta\mathcal{F}|/2c_g$, from which we arrive at our integral momentum balance

$$\left\langle \int_V \rho\overline{u} \, \mathrm{d}V \right\rangle = \frac{1}{2}\frac{|\Delta\mathcal{F}|}{c_g}. \tag{2.10}$$

To make further progress, we now constrain the form of the flow induced by breaking.

2.2. *A model for the mean flow induced by breaking*

Consider the impulse associated with the vorticity induced by breaking, $\boldsymbol{\Omega} = \boldsymbol{\nabla} \times \overline{\boldsymbol{u}}$. The hydrodynamic impulse, $\boldsymbol{I}$, sometimes referred to as Kelvin's impulse (Lamb 1932; Bühler 2007), is defined as

$$\boldsymbol{I} = \frac{1}{2}\rho \left\langle \int_V \boldsymbol{x} \times \boldsymbol{\Omega} \, \mathrm{d}V \right\rangle. \tag{2.11}$$

Note, unlike the momentum of the fluid, the impulse is well defined, as it does not contain the surface integral pressure terms which are not absolutely convergent (Batchelor 1967; Saffman 1992; Bühler 2007).

The rate of change of the impulse is given by

$$\frac{\mathrm{d}\boldsymbol{I}}{\mathrm{d}t} = \int_V \boldsymbol{\mathcal{B}} \, \mathrm{d}V, \tag{2.12}$$

where $\boldsymbol{\mathcal{B}}$ is an impulsive force necessary to instantaneously generate the prescribed flow from rest.

Therefore, the impulse of a given vorticity field can be related to the net force exerted to create it. This allows us to invert the vortex ring problem, and find the impulse, and then the energy, needed to generate this vortical flow from rest, to be compared with the total energy lost by breaking. In particular, we will exploit the relationship between the impulse needed to generate the post-breaking vorticity field and the momentum flux lost by the wave field due to breaking (see also Bühler 2014, § 12.4.2).

However, in order to make progress in solving for this integral $\boldsymbol{I}$, we must constrain the form of the breaking-induced vorticity of the mean flow, i.e. $\boldsymbol{\Omega}$, which we will now do.

Recall, Pizzo & Melville (2013) found that the evolution of the circulation, Γ, of the breaking-induced mean flow can be modelled as

$$\frac{\mathrm{d}\Gamma}{\mathrm{d}t} = \oint_{\mathcal{C}} \boldsymbol{\mathcal{B}} \cdot \mathrm{d}\boldsymbol{\ell}, \tag{2.13}$$

where

$$\Gamma = \oint_{\mathcal{C}} \overline{\boldsymbol{u}} \cdot \mathrm{d}\boldsymbol{\ell}. \tag{2.14}$$

Here, $\mathcal{C}$ is a material contour moving with the mean flow and we recall from above that $\boldsymbol{\mathcal{B}}$ is a parametrization of the breaking-induced body force, responsible for the generation of the mean flow.

There is some choice in how to parameterize the forcing due to breaking, as it is unclear how the final momentum flux of the packet varies as a function of its characteristic initial parameters. Following the laboratory and numerical studies, Pizzo & Melville (2013) sought a function $\boldsymbol{\mathcal{B}}$ that was compact in space and time, had an asymmetry between the x and transverse (y) direction and was also symmetric about this transverse direction.

Based on these constraints, the authors chose to model $\boldsymbol{\mathcal{B}}$ using a thin, impulsively forced half-elliptical disc of semi-major axis A and semi-minor axis B being forced from rest to a speed U along its axis of symmetry, that is in the x-direction, as shown

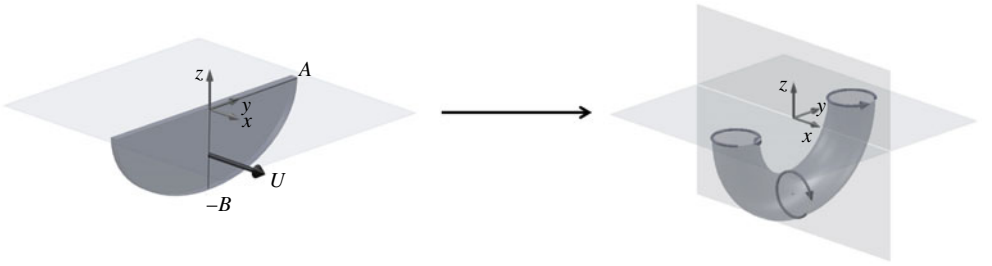

FIGURE 2. A sketch of the bulk scale effects of deep-water breaking on the water column. We assume that breaking acts like a thin impulsively forced disc of semi-major axis A and semi-minor axis B, being forced from rest to a speed U along the x direction. The disc is then assumed to dissolve, with the flow rolling up where it is strongest, that is along its perimeter, leaving a persistent vortex ring that characterizes the ensemble-averaged post-breaking flow.

in figure 2. The disc is assumed to dissolve (Taylor 1953), leaving an elliptical vortex ring, whose properties can be easily related to those of the forced disc.

Dhanak & Bernardinis (1981, Appendix A, see also Pizzo & Melville 2013) found that the impulse, I, of the elliptical disc can be related to the kinetic energy, $\mathbb{T}$, of the generated vortex ring by (cf. (2.11)) $I = 2\mathbb{T}U^{-1}$. This is also consistent with the study of Linden & Turner (2001). We assume this kinetic energy of the disk $\mathbb{T}$ is equivalent to the kinetic energy of the mean flow current $\mathcal{E}_c$.

From (2.10), we can relate the impulse in the mean flow currents to the momentum flux lost by the wave field, and associate this with the impulse needed to generate the mean flow vortex. That is, we find

$$I \equiv \int_V \rho \bar{u}\, \mathrm{d}V = \frac{|\Delta \mathcal{F}|}{2c_g}. \tag{2.15}$$

This allows us to rewrite the kinetic energy of the mean flow as

$$\mathbb{T} = \frac{U|\Delta \mathcal{F}|}{4c_g} = \frac{\Gamma}{8B}\frac{|\Delta \mathcal{F}|}{c_g}, \tag{2.16}$$

where we have substituted in the formula for the circulation of the elliptical vortex ring found by Dhanak & Bernardinis (1981), i.e. $\Gamma = 2UB$.

Finally, we define the central focus of our study. Namely, we consider the ratio of the energy in the breaking-induced vortex to the total energy lost due to breaking, which we define as $\mathcal{R}_c$, and is given by

$$\mathcal{R}_c \equiv \frac{\mathcal{E}_c}{|\Delta \mathcal{F}|} = \frac{\mathbb{T}}{|\Delta \mathcal{F}|} = \frac{\Gamma}{8B}\frac{|\Delta \mathcal{F}|}{c_g|\Delta \mathcal{F}|} = \frac{\Gamma}{4Bc}, \tag{2.17}$$

where the phase velocity is given by $c = \omega/k = 2c_g$ for linear deep-water surface gravity waves.

From Rapp & Melville (1990, see their figure 34), and the scaling arguments of Pizzo & Melville (2013), the depth to which the fluid is mixed, i.e. B, scales with h, which together with (1.2) implies that

$$\mathcal{R}_c = \chi\,(hk)^{1/2}, \tag{2.18}$$

where χ is a constant. We will now examine this quantity using direct numerical simulations of breaking waves.

3. Direct numerical simulations of breaking waves

3.1. *Numerical experiment*

To corroborate our scaling model, we now perform direct numerical simulations (DNS) of the two-dimensional Navier–Stokes equations in a two-phase fluid (air and water) accounting for surface tension and viscous effects using the open source solver Gerris (Popinet 2003, 2009), based on a quad/octree adaptive spatial discretization, multilevel Poisson solver. The interface between the high density liquid (water) and the low density gas (air) is reconstructed by a volume of fluid (VOF) method. This solver has been successfully used in various multiphase problems such as atomization (Fuster *et al.* 2009), the growth of instabilities at the interface (Fuster *et al.* 2013), capillary wave turbulence (Deike *et al.* 2014) and two- and three-dimensional wave breaking (Fuster *et al.* 2009; Deike *et al.* 2015; Deike, Melville & Popinet 2016).

As in Deike *et al.* (2015, 2016), we use nonlinear waves, based on a truncated Stokes expansion, of wavelength λ, as initial conditions to study wave breaking. Note, this method of generating breaking waves is different from the dispersive focusing technique used in the laboratory. This becomes manifest in the value of the breaking threshold. Indeed, as discussed in Deike *et al.* (2015, 2016), the critical slope for wave breaking changes when a steep Stokes wave is used instead of a dispersive focusing packet or a packet undergoing modulational instability. In the present case, a slope of 0.32 corresponds to an incipient breaking wave, which has total dissipation less than a spilling breaker of the same slope obtained by a dispersive wave focusing technique in the laboratory.

In order to simulate the laboratory experiments, the waves must be able to propagate freely after breaking without interfering with the flow created during the breaking event. Thus we consider a two-dimensional (2-D) rectangular numerical domain, with dimension $L = 8\lambda$ in the horizontal propagation direction and $l = \lambda$ in the vertical direction. The mean water level is set at $\eta = 0$, so that the water depth is $d = \lambda/2$. Boundary conditions are periodic in x, but as we will see the main wave never reaches the end of the numerical domain for times necessary to resolve the properties under investigation. The top and bottom walls are free slip (at $z = \pm d = \lambda/2$). The total simulation time corresponds to $8T$, where $T = 2\pi/\omega$ is the wave period and ω the linear angular frequency of the input wave form.

A third-order expansion, based on Stokes waves, is used for the interface $\eta(x, t)$ which together with the velocity potential $\phi(x, z, t)$ in the water constitute the initial conditions at the left of the numerical domain, for $x \in [\lambda/2 : 3\lambda/2]$ and in the rest of the domain, the interface and the velocity are set to 0 by applying a smooth windowing. All cases discussed in this work are single breaking events.

The physical properties of the two phases are those of air and water, and this manifests itself through the density and viscosity ratios. The Bond number is defined as $Bo = \Delta\rho g/(\gamma k^2)$, with $\Delta\rho$ the density difference between the two fluids, and γ is the surface tension, so that Bo gives the ratio between gravity and surface tension forces. The Reynolds number in the water is $Re = c\lambda/\nu$, where $c = \sqrt{g/k}$ is the linear gravity wave phase speed and ν is the kinematic viscosity of the water, which is set to $Re = 40\,000$. This choice is related to spatial resolution constraints, but should not affect the results regarding the wave dissipation, since we are at a sufficiently high Reynolds number (Deike *et al.* 2015, 2016) to capture the phenomena in question. We choose $Bo = 200$ to obtain plunging breakers at high initial wave slope and also to be able to correctly resolve surface tension effects.

We define the characteristic slope to be $S = ak$, with a the initial wave amplitude and $k = 2\pi/\lambda$ the wavenumber. S varies from 0.35 to 0.65, i.e. from non-breaking waves to strongly plunging waves (Deike *et al.* 2015). Note slopes higher than the limiting slope for the full Stokes wave solution can be defined as we are generating our conditions based on a third-order Stokes expansion. It is useful to recall that the slope at breaking is proportional to the initial wave slope in this configuration (Deike *et al.* 2015, 2016), which is consistent with the laboratory findings of the analogous relationship for focusing packets (Drazen *et al.* 2008).

Adaptive mesh refinement is used to accurately solve for the interface and the vortex structures, with a mesh size of $\mathrm{d}x = \mathrm{d}y = \lambda/512$, with adaptive criteria on the vorticity and the interface. This configuration allows accurate solutions for the dissipative scales and surface tension effects, as shown by previous two- and three-dimensional simulations (Deike *et al.* 2015, 2016). As discussed in Deike *et al.* (2015, 2016), this resolution is enough to have full convergence of the DNS and the results presented here are not sensitive to the mesh size. This is achieved thanks to the adaptive methods on the interface and vorticity, and to our choice of Bond number and Reynolds number. Choosing $Bo = 200$ and $Re = 40\,000$ permits us to fully resolve the viscous boundary layer and associated dissipative processes, as well as the surface tension effects, without the use of any subgrid model. Moreover, Deike *et al.* (2015, 2016) showed that this value of the Reynolds number is high enough to reproduce the dissipative properties that were observed in the laboratory results; and Deike *et al.* (2015) showed that the dissipation for breaking waves of slopes $S > 0.35$ is not sensitive to the Bond number for $Bo > 100$. This validates our choice of physical parameters and mesh grid size for the present study.

Note, we find that for the breaking waves modelled in this paper, the energy dissipated in the water column dominates (i.e. is more than 96 % of the total energy lost by the wave field, in all tested cases) the energy dissipated in the air. This is consistent with the fact that the density of the water is several orders of magnitude larger than that of the air and agrees with laboratory studies on air flow over breaking waves (Banner & Melville 1976; Veron, Saxena & Misra 2007; Belden & Techet 2011).

A typical DNS evolution of a breaking wave, with $S = 0.55$, is shown in figure 3. The wave propagates from the left to the right before undergoing strongly nonlinear behaviour leading to breaking. A jet is formed at the front of the wave that subsequently impacts the water surface. The time of the breaking event, or impact with the surface, t_b, occurs between $t/T = 0.5$ and $t/T = 1$, as in Deike *et al.* (2015, 2016), while the jet impacts the free surface at approximately $x_b = x/\lambda \approx 2.5$. Figure 3 shows that the breaking event generates turbulent motion and strong vortical structures in the water in the area bounded by $x \in [2.5 : 3.5]\lambda$. This defines the breaking area. After breaking, the waves are transmitted and radiated from the breaking region, subsequently rendering the free surface as a rigid lid in this area, which is consistent with the laboratory studies and figure 1. However, the breaking-induced current, characterized by the vortex, is still present in the breaking region several periods after t_b.

Here, we focus on post-breaking flow properties and the resulting vorticity, and its associated circulation, as well as the kinetic energy flux of the current in the breaking area, for long times after the waves have propagated away.

As was discussed above, the generated vortical structure has been observed experimentally and was found to be a coherent vortex by Rapp & Melville (1990),

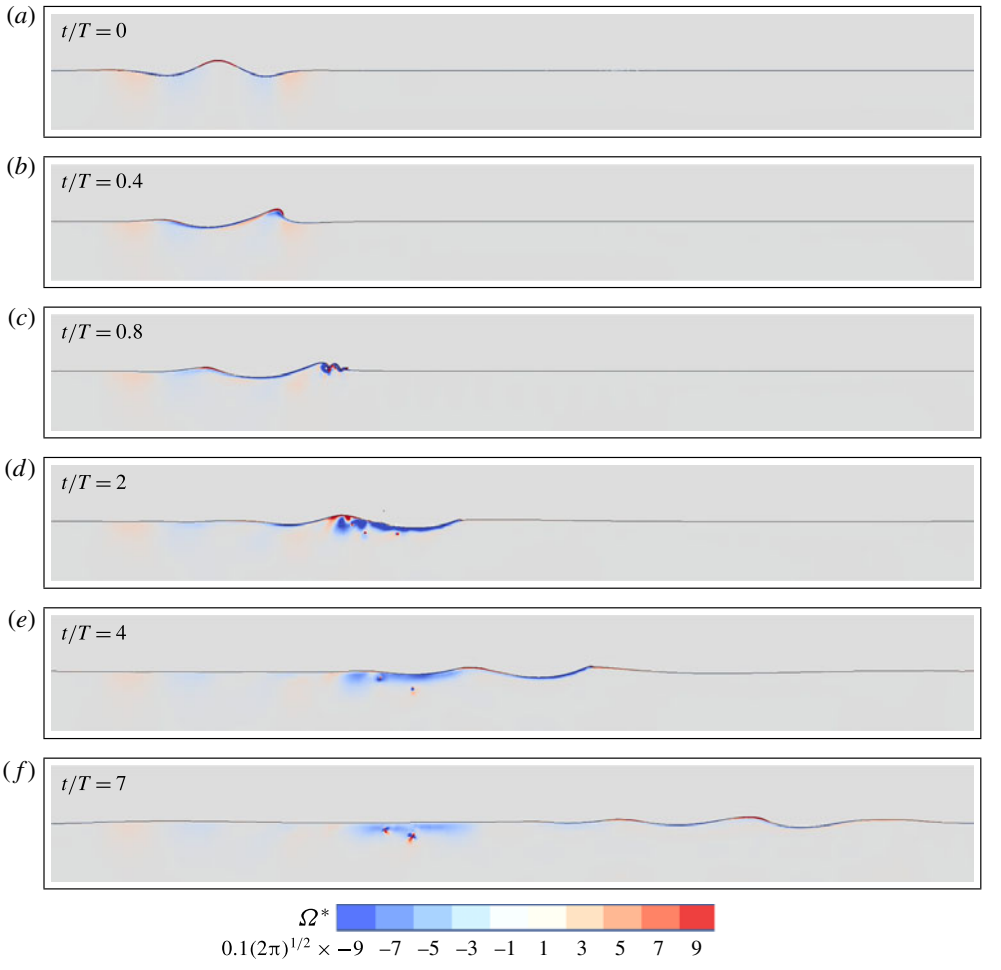

FIGURE 3. Time evolution of a plunging breaker with the vorticity field $\Omega^* = \Omega/\omega$ at different time steps. The wave starts at the left of the numerical domain, propagates to the right and breaks after half a period of propagation. The waves then propagate out of the region where breaking occurred, leaving an active vorticity field that characterizes the post-breaking flow. The initial conditions were chosen such that $S = 0.55$, $Re = 4 \times 10^4$, $Bo = 200$.

Melville *et al.* (2002), which was described in more detail by Pizzo & Melville (2013). Figure 4 shows a close up of this area several periods after breaking. A coherent vortex is indeed observed and remains stable, slowly moving towards the right of the numerical domain. Its intensity slowly decreases due to viscous dissipation, consistent with Melville *et al.* (2002). Recall, Ω^* is the vorticity field normalized by the characteristic angular frequency ω, in the y direction.

3.2. *Energy dissipated by breaking, circulation and mean currents*

We now calculate the integral properties of the breaking waves for various slopes S. To begin, we compute the energy flux $\mathcal{F}$, i.e. equation (2.5), by relating this to the

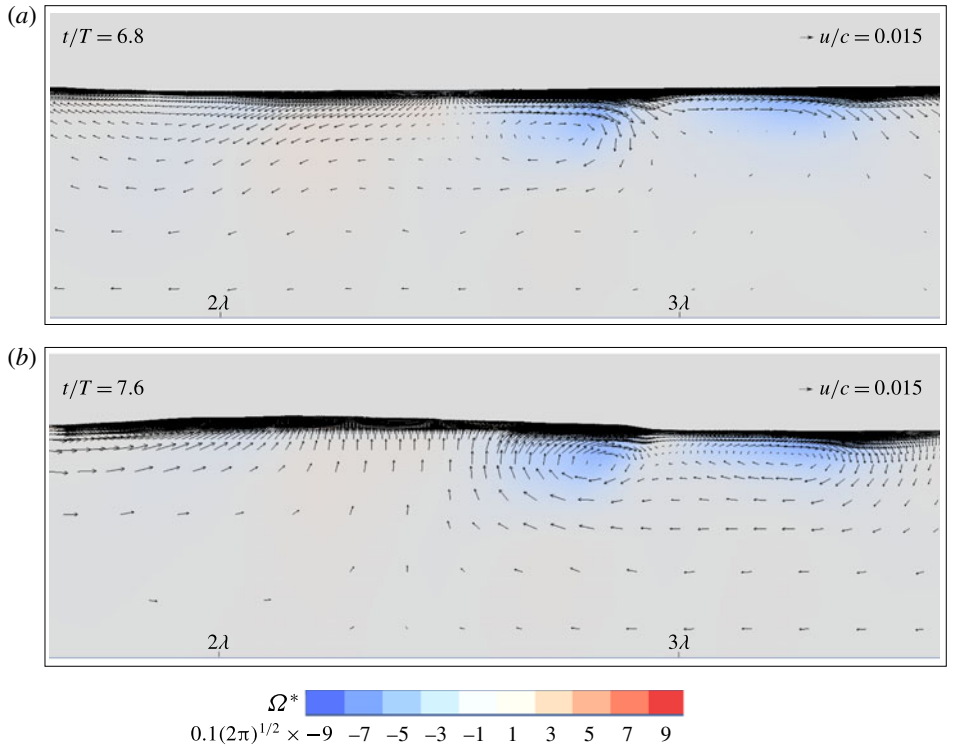

FIGURE 4. The normalized vorticity field Ω^* remaining in the region after a plunging breaker, and after the remaining waves have propagated away. The post-breaking flow is characterized by a compact region of vorticity, outside of which the flow is largely irrotational. $Re = 4 \times 10^4$, $Bo = 200$ and $S = 0.5$.

energy density, E, through linear theory (far upstream and downstream of the breaking event), where

$$E = \left\langle \int_0^{\mathcal{T}_0} \frac{1}{2}\rho g \eta^2 \, \mathrm{d}t \right\rangle . \tag{3.1}$$

That is, the energy flux at a given location is then $\mathcal{F}(x) = c_g E(x)$ where $c_g = (1/2)c$ is the group velocity of the wave and c is the phase speed. As defined in § 2, the change in energy flux due to breaking is then given by $\Delta\mathcal{F} = c_g \Delta E$. Note, following the laboratory experiments of Drazen *et al.* (2008), this relation assumes that the group velocity is approximately equal before and after breaking (see also Pizzo & Melville 2016). The dissipated energy flux per unit length of breaking crest ϵ_l is then given by $\epsilon_l = |\Delta\mathcal{F}|/\tau_b$, where τ_b is the active breaking time and in these experiments it is found that $\tau_b \approx T$ which is consistent with other laboratory (Drazen *et al.* 2008) and numerical studies (Deike *et al.* 2015, 2016).

Figure 5(*a*) shows the breaking parameter b as a function of the slope S in the DNS and in available laboratory data. The breaking parameter b as a function of the slope S in the present DNS is found in good agreement with previous experimental results and the semi-empirical model of Drazen *et al.* (2008, see also Grare *et al.* (2013)) and Romero *et al.* (2012) for strong breaking waves, as in our previous

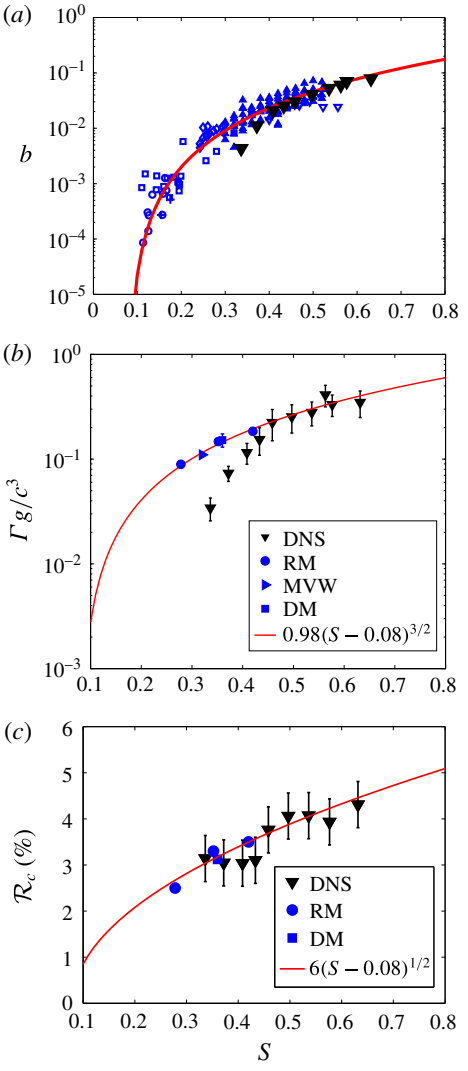

FIGURE 5. In all three plots, (▼) are DNS data. (*a*) Breaking parameter b as a function of the initial wave slope S. Solid line: semi-empirical formulation based on scaling argument, $b = 0.4(S - 0.08)^{5/2}$ (Romero *et al.* 2012). Blue symbols are experimental data; triangles and diamonds are from Drazen *et al.* (2008), cross and circle are from Banner & Peirson (2007) and squares are from Grare *et al.* (2013). The differences between experiments and DNS at lower values of S come from differences in initiating wave breaking. (*b*) Circulation generated by the breaking event Γ (normalized by c^3/g) as a function of S. Solid line is the model from Pizzo & Melville (2013) fitted to experimental data, $\Gamma g/c^3 = \gamma_0(S - S_0)^{3/2}$, where $\gamma_0 = 0.98$ and $S_0 = 0.08$. Blue closed circles are from Rapp & Melville (1990), the right triangle is from Melville *et al.* (2002) and the square is from Drazen & Melville (2009). (*c*) Ratio of the energy flux in the current (created by the breaking event) and the dissipated energy flux due to the breaking wave, $\mathcal{R}_c$. Blue closed circles (RM): laboratory data from Rapp & Melville (1990); closed blue square (DM) is a data point from Drazen & Melville (2009). Solid line is $\mathcal{R}_c = \mathcal{E}_c/|\Delta F| = \chi(S - S_0)^{1/2}$ based on the model presented in § 2, equation (2.18) and including an empirical threshold slope, equation (3.2), with $S_0 = 0.08$ and $\chi = 0.06$ the best fit to the data.

numerical work (Deike *et al.* 2015, 2016). The difference in the dissipation between experiments and DNS for S between 0.35 and 0.4 is most likely related to the route to breaking, i.e. how the initial conditions are chosen. Indeed, as discussed in Deike *et al.* (2015, 2016), the critical slope for wave breaking changes when a steep Stokes wave is used instead of a dispersive focusing packet or a packet undergoing modulational instability. In the present case, a slope of 0.32 corresponds to an incipient breaking wave, which has total dissipation less than a spilling breaker of the same slope obtained by a dispersive wave focusing technique in the laboratory. Note, other numerical studies have examined the dissipation due to breaking waves and have found results compatible with the one presented here and in Deike *et al.* (2015, 2016) (see the two-dimensional DNS of Iafrati 2011), and the two- and three-dimensional large eddy simulation (LES) of Derakhti & Kirby (2014), Lubin & Glockner (2015), and Derakhti & Kirby (2016).

The integrated vorticity and the kinetic energy flux over the breaking area are approximately constant with time, slowly decreasing due to viscous dissipative effects, which is consistent with the laboratory studies of Melville *et al.* (2002). The circulation Γ given by (2.14), is averaged over two wave periods, starting four wave periods after the breaking event when the waves have propagated out of the region of breaking. The error bars on Γ in the DNS are representative of its sensitivity to the area and time of integration.

Figure 5(*b*) shows Γ as a function of the wave slope, compared to the limited available laboratory data and the corresponding scaling from Pizzo & Melville (2013) for the circulation, $\Gamma = \gamma_0(S - S_0)^{3/2}$, where γ_0 is an order-one constant and S_0 is the threshold for breaking. The experimental data presented in figure 5(*b*) are from the laboratory studies of Rapp (1986), Rapp & Melville (1990), Melville *et al.* (2002), Drazen & Melville (2009), who computed either explicitly the circulation or provided the measurements of the velocity fields. This is discussed in detail in Pizzo & Melville (2013). The constant $\gamma_0 = 0.98$ was found by a best fit with the data presented in Pizzo & Melville (2013) and shown by the blue circles in 5(*b*), while $S_0 = 0.08$ is the threshold that best fits multiple laboratory studies, as discussed in Romero *et al.* (2012). Good agreement is found between the model for Γ and the available experimental data and the numerical results for large values of S. This is consistent with the findings of Deike *et al.* (2015, 2016) for the energy dissipation rate, where as mentioned above it is noticed that the different breaking generation methods between the laboratory and the numerical experiments are manifest in the breaking threshold parameter S_0.

Finally, figure 5(*c*) shows the main result of this paper, namely the ratio of the energy flux transferred to the current to the dissipated energy flux due to the breaking wave, i.e. $\mathcal{R}_c$. Note, following the laboratory studies of (Melville *et al.* 2002), and consistent with the theoretical assumptions made in § 2, we have assumed that the energy remaining in the region of breaking is entirely in the mean flow. Figure 5(*c*) shows $\mathcal{R}_c$ as a function of the wave slope in the present DNS, together with the experimental data from Rapp & Melville (1990), Drazen & Melville (2009) (note that Melville *et al.* (2002) provided a measure of Γ; however, they did not provide a measure of $\mathcal{E}_c$). The data are well described by the scaling given by (2.18), including the breaking threshold,

$$\mathcal{R}_c = \chi\,(S - S_0)^{1/2}, \tag{3.2}$$

with $\chi = 0.06$ and $S_0 = 0.08$ is the critical slope determined by Romero *et al.* (2012). The value $\chi = 0.06$ is the least-squares fit to the laboratory and numerical data.

Note that there is a physical relation between Γ and $\mathcal{E}_c$, and dimensionally we get $\mathcal{E}_c \propto \rho\Gamma^2$. This allows us to perform a consistency check on our relationship given in (2.18). Namely, we have ensured that values of b, consistent with the laboratory and numerical data, can be retrieved from Γ and $\mathcal{R}_c$, where $\mathcal{R}_c \propto (\Gamma g/c^3)^2/b$.

We find that $\mathcal{R}_c$ varies from 2 % to 5 % for slopes corresponding to incipient breaking waves to strong plunging events, in good agreement with the earlier experimental results from Rapp & Melville (1990) as well as an additional point from the laboratory data of Drazen & Melville (2009). Note, the number of these measurements that is available is limited, as one must measure the kinetic energy in the region of breaking several wave periods after the breaking event. This is why there are far fewer measurements of this quantity versus, for example, the energy dissipation rate per unit length of breaking crest ϵ_l. The scatter in the numerical data comes from the difficulties in properly estimating a small difference between two large quantities (energy flux before and after breaking) and the fact that the ratio $\mathcal{R}_c$ is a small quantity. Finally the agreement with the scaling argument presented in § 2 is encouraging. In the next section, we discuss some of the implications of these results.

4. Discussion

In this study we have proposed a simple model for the energy transferred from the wave field to the mean flow by wave breaking. This serves as another study (Drazen *et al.* 2008; Romero *et al.* 2012; Pizzo & Melville 2013; Deike *et al.* 2015) that uses simple scaling arguments (with the relevant parameter being the local slope at breaking S) to describe integral properties associated with wave breaking. That is, S, which is known *a priori* and is related to the energy available to the water column due to breaking, is the primary variable that characterizes integral properties of the post-breaking flow field.

What is perhaps surprising is that for such a complex turbulent flow as wave breaking, so much information can be teased out of a relatively simple vortex dynamics model, or equivalently, that the vortex dynamics has such a constraint on the overall dynamics of the flow. If sustained by further experimental and numerical support, the results of this paper provide the beginnings of the answer to the question: How is the energy lost from a wave field due to breaking distributed between currents and turbulence? The results suggest that only a very small fraction of that energy is available for generating currents, the rest going into local turbulence and mixing of the near-surface waters.

Ocean currents can be generated by a variety of phenomena, including tidal forcing, buoyancy gradients, wind drift, the irrotational wave-induced mean flow (i.e. Stokes drift) and wave breaking. This paper has focused on the last effect, as it is believed that wave breaking is the dominant contribution to the wind-driven currents. In particular, for wind speeds above (6–8) m s^{-1}, the momentum and energy from the atmosphere are mainly transmitted through the wave field, with nearly 100 % of these quantities being passed directly to the water column through the action of wave breaking (Terray *et al.* 1996; Banner & Peirson 1998; Donelan 1998; Sullivan *et al.* 2007; Sullivan & McWilliams 2009). That is, just a small amount of energy is radiated away in the form of surface waves. We have found that most of the energy lost locally from the wave field (at least 95 % for the waves considered in this paper) is dissipated through turbulence, with the remainder going into the breaking-induced mean flow.

Phillips (1985) proposed that a statistical description of wave breaking could be used to deduce bulk scale features of the saturation range of the surface wave field (where, by definition, 100 % of the wind input is passed locally to the water column), including the total energy dissipated by the wave field due to breaking. This description relies crucially on the statistical distribution of breaking, as a function of the variables characterizing the local ocean and atmospheric conditions. In a recent paper, Sutherland & Melville (2013), using a scaling argument motivated by field data, took the relevant variables to be the atmospheric friction velocity, the significant wave height, the phase velocity of the waves at the peak of the wind–wave spectrum and gravity. The resulting form of the probability distribution function for wave breaking based on these variables was found to collapse the existing field data onto a single curve.

Therefore, the framework derived in this paper could be extended, in the spirit of Romero *et al.* (2012), to give a spectral statistical description of the energy transferred to the mean flow due to wave breaking in a wind–wave model. This would also be important for constraining global energy budgets in more sophisticated wave resolving ocean–atmosphere models (Sullivan *et al.* 2007; Cavaleri *et al.* 2012).

Acknowledgements

This research was supported by grants to W.K.M. from NSF (OCE) and ONR (Physical Oceanography).

REFERENCES

BANNER, M. L. & MELVILLE, W. K. 1976 On the separation of air flow over water waves. *J. Fluid Mech.* **77** (04), 825–842.

BANNER, M. L. & PEIRSON, W. L. 2007 Wave breaking onset and strength for two-dimensional deep-water wave groups. *J. Fluid Mech.* **585**, 93–115.

BANNER, M. L. & PEIRSON, W. L. 1998 Tangential stress beneath wind-driven air–water interfaces. *J. Fluid Mech.* **364**, 115–145.

BATCHELOR, G. K. 1967 *An Introduction to Fluid Dynamics*. Cambridge University Press.

BELDEN, J. & TECHET, A. H. 2011 Simultaneous quantitative flow measurement using PIV on both sides of the air–water interface for breaking waves. *Exp. Fluids* **50** (1), 149–161.

BÜHLER, O. 2007 Impulsive fluid forcing and water strider locomotion. *J. Fluid Mech.* **573**, 211–236.

BÜHLER, O. 2014 *Waves and Mean Flows*. Cambridge University Press.

CAVALERI, L., FOX-KEMPER, B. & HEMER, M. 2012 Wind waves in the coupled climate system. *Bull. Am. Meteorol. Soc.* **93** (11), 1651–1661.

DEIKE, L., FUSTER, D., BERHANU, M. & FALCON, E. 2014 Direct numerical simulations of capillary wave turbulence. *Phys. Rev. Lett.* **112**, 234501.

DEIKE, L., MELVILLE, W. K. & POPINET, S. 2016 Air entrainment and bubble statistics in breaking waves. *J. Fluid Mech.* **801**, 91–129.

DEIKE, L., POPINET, S. & MELVILLE, W. 2015 Capillary effects on wave breaking. *J. Fluid Mech.* **769**, 541–569.

DERAKHTI, M. & KIRBY, J. T. 2014 Bubble entrainment and liquid–bubble interaction under unsteady breaking waves. *J. Fluid Mech.* **761**, 464–506.

DERAKHTI, M. & KIRBY, J. T. 2016 Breaking-onset, energy and momentum flux in unsteady focused wave packets. *J. Fluid Mech.* **790**, 553–581.

DHANAK, M. R. & BERNARDINIS, B. 1981 The evolution of an elliptic vortex ring. *J. Fluid Mech.* **109**, 189–216.

DONELAN, M. A. 1998 Air–water exchange processes. *Coast. Estuar. Stud.* 19–36.

DRAZEN, D. A. & MELVILLE, W. K. 2009 Turbulence and mixing in unsteady breaking surface waves. *J. Fluid Mech.* **628**, 85–119.

DRAZEN, D. A., MELVILLE, W. K. & LENAIN, L. 2008 Inertial scaling of dissipation in unsteady breaking waves. *J. Fluid Mech.* **611**, 307–332.

DUNCAN, J. H. 1981 An experimental investigation of breaking waves produced by a towed hydrofoil. *Proc. R. Soc. Lond.* A **377** (1770), 331–348.

FUSTER, D., AGBAGLAH, G., JOSSERAND, C., POPINET, S. & ZALESKI, S. 2009 Numerical simulation of droplets, bubbles and waves: state of the art. *Fluid Dyn. Res.* **41**, 065001.

FUSTER, D., MATAS, J.-P., MARTY, S., POPINET, S., HOEPFFNER, J., CARTELLIER, A. & ZALESKI, S. 2013 Instability regimes in the primary breakup region of planar coflowing sheets. *J. Fluid Mech.* **736**, 150–176.

GRARE, L., PEIRSON, W. L., BRANGER, H., WALKER, J. W., GIOVANANGELI, J.-P. & MAKIN, V. 2013 Growth and dissipation of wind-forced, deep-water waves. *J. Fluid Mech.* **722**, 5–50.

IAFRATI, A. 2011 Energy dissipation mechanisms in wave breaking processes: spilling and highly aerated plunging breaking events. *J. Geophys. Res.* **116** (C7), doi:10.1029/2011JC007038.

LAMB, H. 1932 *Hydrodynamics*. Cambridge University Press.

LINDEN, P. F. & TURNER, J. S. 2001 The formation of 'optimal' vortex rings, and the efficiency of propulsion devices. *J. Fluid Mech.* **427**, 61–72.

LONGUET-HIGGINS, M. S. & STEWART, R. W. 1964 Radiation stresses in water waves; a physical discussion, with applications. In *Deep Sea Research and Oceanographic Abstracts*, vol. 11, pp. 529–562. Elsevier.

LUBIN, P. & GLOCKNER, S. 2015 Numerical simulations of three-dimensional breaking waves: aeration and turbulent structures. *J. Fluid Mech.* **767**, 364–393.

MCINTYRE, M. E. 1981 On the wave momentum myth. *J. Fluid Mech.* **106**, 331–347.

MEI, C. C. 1989 *The Applied Dynamics of Ocean Surface Waves*. vol. 1. World Scientific.

MELVILLE, W. K. 1996 The role of surface-wave breaking in air-sea interaction. *Annu. Rev. Fluid Mech.* **28** (1), 279–321.

MELVILLE, W. K. & FEDOROV, A. V. 2015 The equilibrium dynamics and statistics of gravity–capillary waves. *J. Fluid Mech.* **767**, 449–466.

MELVILLE, W. K., VERON, F. & WHITE, C. J. 2002 The velocity field under breaking waves: coherent structure and turbulence. *J. Fluid Mech.* **454**, 203–233.

PEREGRINE, D. H. 1999 Large-scale vorticity generation by breakers in shallow and deep water. *Eur. J. Mech. (*B*/Fluids)* **18** (3), 403–408.

PHILLIPS, O. M. 1977 *The Dynamics of the Upper Ocean*. Cambridge University Press.

PHILLIPS, O. M. 1985 Spectral and statistical properties of the equilibrium range in wind-generated gravity waves. *J. Fluid Mech.* **156**, 505–531.

PIZZO, N. E. & MELVILLE, W. K. 2016 Wave modulation: the geometry, kinematics and dynamics of surface-wave focusing. *J. Fluid Mech.* (in press).

PIZZO, N. E. & MELVILLE, W. K. 2013 Vortex generation by deep-water breaking waves. *J. Fluid Mech.* **734**, 198–218.

POPINET, S. 2003 Gerris: a tree-based adaptative solver for the incompressible Euler equations in complex geometries. *J. Comput. Phys.* **190**, 572–600.

POPINET, S. 2009 An accurate adaptative solver for surface-tension-driven interfacial flows. *J. Comput. Phys.* **228**, 5838–5866.

RAPP, R. J. & MELVILLE, W. K. 1990 Laboratory measurements of deep-water breaking waves. *Phil. Trans. R. Soc. Lond.* A 735–800.

RAPP, R. J. 1986 Laboratory measurements of deep water breaking waves. PhD thesis, Massachusetts Institute of Technology.

ROMERO, L., MELVILLE, W. K. & KLEISS, J. M. 2012 Spectral energy dissipation due to surface wave breaking. *J. Phys. Oceanogr.* **42**, 1421–1441.

SAFFMAN, P. G. 1992 *Vortex Dynamics*. Cambridge University Press.

SULLIVAN, P. P. & MCWILLIAMS, J. C. 2009 Dynamics of winds and currents coupled to surface waves. *Annu. Rev. Fluid Mech.* **42**, 19–42.

SULLIVAN, P. P., MCWILLIAMS, J. C. & MELVILLE, W. K. 2004 The oceanic boundary layer driven by wave breaking with stochastic variability. Part 1. Direct numerical simulations. *J. Fluid Mech.* **507**, 143–174.

SULLIVAN, P. P., MCWILLIAMS, J. C. & MELVILLE, W. K. 2007 Surface gravity wave effects in the oceanic boundary layer: Large-eddy simulation with vortex force and stochastic breakers. *J. Fluid Mech.* **593**, 405–452.

SUTHERLAND, P. & MELVILLE, W. K. 2013 Field measurements and scaling of ocean surface wave-breaking statistics. *Geophys. Res. Lett* **40** (12), 3074–3079.

TAYLOR, G. I. 1953 Formation of a vortex ring by giving an impulse to a circular disk and then dissolving it away. *J. Appl. Phys.* **24** (1), 104.

TERRAY, E. A., DONELAN, M. A., AGRAWAL, Y. C., DRENNAN, W. M., KAHMA, K. K., WILLIAMS, A. J., HWANG, P. A. & KITAIGORODSKII, S. A. 1996 Estimates of kinetic energy dissipation under breaking waves. *J. Phys. Oceanogr.* **26** (5), 792–807.

TIAN, Z., PERLIN, M. & CHOI, W. 2011 Frequency spectra evolution of two-dimensional focusing wave groups in finite depth water. *J. Fluid Mech.* **688**, 169–194.

VERON, F., SAXENA, G. & MISRA, S. K. 2007 Measurements of the viscous tangential stress in the airflow above wind waves. *Geophys. Res. Lett.* **34** (19).